
LiteMedCoT-VL: Parameter-Efficient Adaptation for Medical Visual Question Answering

Runze Ma

School of Information Technology
Monash University Malaysia
rmaa0033@student.monash.edu

Shunbo Jia

Faculty of Innovation Engineering
Macau University of Science and Technology
2240003657@student.must.edu.mo

Haonan Lyu

Department of Bioelectronics
Faculty of Biomedical Engineering
Shenzhen University of Advanced Technology
SUAT25060153@stu.suat-sz.edu.cn

Guo Liu

School of Mathematics and Statistics
Huazhong University of Science and Technology
u202210024@hust.edu.cn

Caizhi Liao*

Department of Bioelectronics
Faculty of Biomedical Engineering
Shenzhen University of Advanced Technology
liaocaizhi@suat-sz.edu.cn

Abstract

The reasoning gap between large and compact vision-language models (VLMs) limits the deployment of medical AI on portable clinical devices. Compact VLMs of 2–4B parameters can run on resource-constrained hardware but lack the multi-step reasoning capacity needed for interpretable clinical decision support. Existing knowledge distillation methods transfer answers without the reasoning process behind them. Medical visual question answering (VQA) serves as a testbed for this problem, as it requires models to integrate visual evidence with clinical knowledge through structured reasoning chains. We introduce LiteMedCoT-VL, a pipeline that transfers chain-of-thought reasoning from a 235B teacher model to 2B student models through LoRA-based fine-tuning on explanation-enriched training data. All inference is conducted without image captions by default, simulating the clinical scenario in which a physician interprets a medical image directly without an accompanying radiology report. On the PMC-VQA benchmark, LiteMedCoT-VL achieves 64.9% accuracy, exceeding the zero-shot Qwen3-VL-4B baseline of 53.9% by 11.0 percentage points and outperforming all published baselines. This result indicates that a 2B model with reasoning distillation can match or exceed models with twice the parameters. Visual grounding analysis shows that the model relies on image content rather than exploiting textual priors. Our code is publicly available at <https://anonymous.4open.science/r/LiteMedCoT-VL>.

*Corresponding author.

1 Introduction

Medical imaging has progressed from handcrafted features to deep learning and, more recently, to systems that combine visual evidence with language understanding [1–3]. Vision-language models (VLMs) trained on large image–text collections perform well on new tasks without task-specific training [4–7], and adapting these models for medical image question answering is an active research area [8–10].

Deploying these models on portable medical devices presents a fundamental challenge. Large VLMs achieve strong performance but require computing resources that exceed the capacity of portable imaging equipment and clinical devices with limited hardware. Compact models with 2–4B parameters can run on such hardware but often lack the multi-step reasoning capacity needed for clinical decision support. Knowledge distillation transfers abilities from a large model to a smaller one [11, 12], yet conventional distillation methods transfer only answer labels without the reasoning process behind them.

Recent work has begun to address this gap through structured chain-of-thought (CoT) annotations [13, 14], reinforcement learning with process rewards [15], agentic grounding frameworks [16], and preference-based optimization [17]. These approaches demonstrate that transferring reasoning capability, rather than answer patterns alone, improves medical VQA performance. However, they often require expert-annotated reasoning traces, complex multi-stage training pipelines, or substantial additional compute. A simpler recipe that distills reasoning from a large teacher into a compact student via parameter-efficient fine-tuning remains underexplored.

This work introduces LiteMedCoT-VL, a pipeline that adapts compact vision-language models for medical visual question answering through chain-of-thought knowledge distillation and LoRA-based fine-tuning. A large teacher model generates step-by-step clinical reasoning chains, which are injected into the training data to transfer reasoning patterns to a compact student model. The PMC-VQA benchmark [18] serves as our evaluation platform.

Our contributions are as follows.

- We present LiteMedCoT-VL, a pipeline that transfers chain-of-thought reasoning from a large vision-language model to compact models through parameter-efficient fine-tuning.
- We show that chain-of-thought distillation from Qwen3-VL-235B-A22B-Instruct [19] improves the accuracy of a 2B parameter student model from 48.7% to 64.9% on PMC-VQA.
- We report experimental results comparing our approach against published baselines and compact open-source models, demonstrating that our best configuration outperforms all existing methods on this benchmark.

2 Related Work

Medical image analysis has progressed through a sequence of paradigm shifts over the past two decades. Early approaches relied on thresholding, edge detection, and handcrafted feature representations [20, 21]. The adoption of convolutional neural networks (CNNs) in the 2010s brought substantial improvements in classification and segmentation accuracy [22–24], and the subsequent introduction of Transformers further advanced global-context modeling for medical imagery [25–27]. Building on these advances, multimodal approaches that integrate visual evidence with language context emerged as a natural next step, demonstrating strong results across medical imaging tasks [1, 3].

This progression gave rise to VLMs that combine visual encoders with language models, enabling image-grounded question answering and report generation [7, 28]. Early vision-language pretraining established the foundation through contrastive learning on large-scale image-text collections [4, 5], followed by unified architectures that process both modalities within a single framework [29, 30]. Medical-focused systems adapted these general-purpose models for clinical applications: LLaVA-Med [31] and MedICaP [18] demonstrated promising results on benchmarks such as SLAKE [32], PathVQA [33], and VQA-Med [34]. However, the strongest performance consistently came from very large models exceeding 70B parameters, which cannot run on the compute and memory capacity of portable medical devices. This growing gap between model capability and deployability motivated a parallel line of work on model compression and efficient adaptation.

As VLMs grew larger, knowledge distillation emerged as a primary strategy for compressing large models into smaller ones while preserving performance [11, 12]. Early methods matched output distributions or intermediate representations between teacher and student [35, 36], and have been widely applied in the medical domain to compress models while preserving diagnostic accuracy [37]. In parallel, compact vision-language models were developed with efficient architectures suitable for resource-constrained deployment, including Phi-3.5-vision [38], InternVL2 [39], and SmolVLM2 [40]. Despite these efficiency gains, compact models still lacked the multi-step reasoning capacity of larger systems, creating a need for methods that could transfer reasoning capability rather than just answer patterns.

This need led to combining distillation with chain-of-thought reasoning [41], which generates step-by-step explanations that make clinical reasoning explicit. When trained on these explanations, the student model learns not just the correct answer but the reasoning process behind it [42, 43], an approach particularly relevant for medical tasks where interpretable reasoning is as important as the final prediction. Step-CoT [13] extends this idea with expert-curated, structured multi-step CoT annotations aligned to clinical diagnostic workflows, coupled with a dynamic graph-structured focusing mechanism. CheXthought [14] provides a large-scale dataset of CoT reasoning traces with synchronized visual attention annotations from hundreds of radiologists, demonstrating that models trained on these traces surpass VLM-generated CoT in factual accuracy and spatial grounding. MedE2 [17] proposes a two-stage pipeline that first elicits multimodal reasoning via orchestrated demonstrations and then enhances it with Direct Preference Optimization. Beyond supervised and preference-based methods, reinforcement learning approaches have emerged: trajectory-aware GRPO [15] applies process rewards based on reasoning-step similarity, and CARE [16] decomposes medical VQA into specialized sub-modules trained with reinforcement learning with verifiable rewards. These methods demonstrate that reasoning capability can be transferred through diverse mechanisms, though they often require expert annotations, complex multi-stage pipelines, or substantial additional compute.

Full fine-tuning of large foundation models also became impractical in memory and compute, motivating parameter-efficient alternatives. LoRA [44] injects trainable low-rank matrices into attention projections, updating less than 1% of parameters while preserving pretrained capabilities. Subsequent work introduced adapters [45], prompt tuning [46], and hybrid strategies [47] to further reduce adaptation cost. In medical settings, these methods enable model customization under the resource constraints of clinical hardware [48, 49]. Our approach combines LoRA with chain-of-thought distillation, transferring reasoning capability from a 235B teacher to a 2B student through a simpler, single-stage recipe that does not require expert-annotated reasoning traces.

A growing body of work examines whether medical vision-language models genuinely ground their reasoning in visual evidence. MIRAGE [50] demonstrates that models can perform competitively on medical VQA benchmarks even when images are withheld, raising concerns about textual prior exploitation. MedVR [51] proposes annotation-free visual reasoning through agentic reinforcement learning with entropy-guided visual regrounding. ViTAR [52] introduces an iterative think-act-rethink chain that treats medical images as interactive objects, with visual attention analysis showing that reasoning rounds increasingly anchor to clinically critical regions. DCI [53] addresses confounding biases through a causal framework that disentangles true causal effects from spurious cross-modal shortcuts. Zafar et al. [54] propose counterfactual evaluation using real, blank, and shuffled images, introducing metrics such as Visual Reliance Score (VRS), Image Sensitivity (IS), and Hallucinated Visual Reasoning Rate (HVRR) to measure genuine visual dependence. HALT-MedVQA [55] constructs hallucination stress tests through fake questions, “None of the Above” choices, and mismatched image substitutions. Additional factors affecting medical VLM reliability include resolution sensitivity [56] and multi-image reasoning demands [57]. These findings motivate our visual grounding analysis as a necessary complement to accuracy reporting.

3 Methodology

3.1 Pipeline Overview

LiteMedCoT-VL adapts compact vision-language models for medical visual question answering through chain-of-thought knowledge distillation and parameter-efficient fine-tuning. Figure 1 provides an overview of the pipeline. It consists of three stages. First, a large teacher model generates chain-of-thought explanations for training samples. Second, these explanations are injected into the

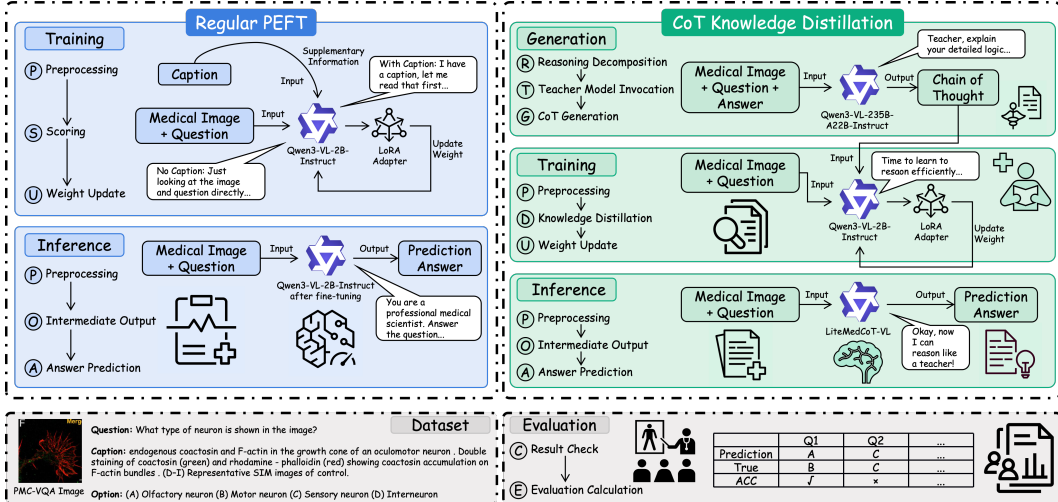


Figure 1: Overview of the LiteMedCoT-VL pipeline. Training samples are processed through prompt engineering, chain-of-thought explanation generation from a large teacher model, and LoRA-based fine-tuning of compact student models.

training data. Third, the compact student model is fine-tuned using LoRA on the enriched dataset. Model adaptation applies LoRA to the query, key, value, and output projections (q_proj , k_proj , v_proj , o_proj) with rank $r = 32$, scaling factor $\alpha = 64$, and dropout rate 0.05. These LoRA modules are inserted into every attention layer of the language model backbone, while the vision encoder remains frozen. Freezing the vision encoder preserves the pretrained visual representations and reduces the number of trainable parameters, which is critical under the memory constraints of portable deployment. The full pipeline uses standardized prompts and deterministic evaluation.

3.2 Prompt Design and Inference

The pipeline uses two core prompt families for answer-only inference and a third for chain-of-thought training. All prompts enforce strict output formatting to eliminate parsing ambiguity; the exact prompt texts are provided in Appendix A.1.

Our primary evaluation protocol provides the model with only the image and question, requiring it to output a single uppercase letter without explanation. We adopt this no-caption setting as the default because it simulates the clinical workflow in which a physician interprets a medical image directly from visual evidence, without an accompanying radiology report. This scenario is common in primary care, emergency departments, and point-of-care settings where a formal written report is not immediately available.

The no-caption setting also provides a more rigorous evaluation. Caption text may contain answer-relevant cues that shortcut visual reasoning, inflating accuracy without genuine image understanding. In PMC-VQA specifically, captions can correlate with answer labels, creating a risk of data leakage. By defaulting to no-caption inference, we ensure that reported performance reflects visual reasoning rather than textual priors. Caption-aware results serve as an upper-bound reference and are reported in the ablation study (Section 5).

We employ next-token probability scoring rather than autoregressive generation to eliminate decoding stochasticity. For each sample, the model processes the image and prompt, and we extract logits at the final token position for the four candidate labels A, B, C, and D, including both bare and space-prefixed tokenizations. The label with the highest logit is selected as the prediction. This approach ensures deterministic, reproducible evaluation.

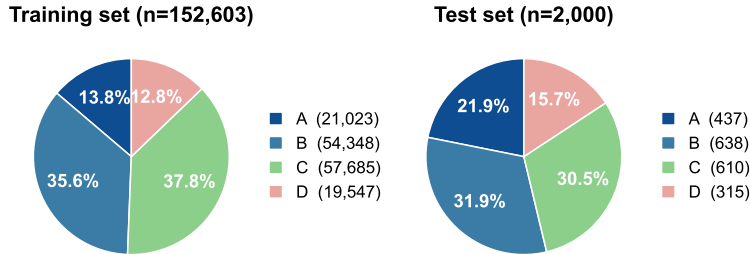


Figure 2: Answer label distribution in the PMC-VQA training and test sets. Options B and C dominate both splits, accounting for 73.5% of training and 62.4% of test samples.

4 Experiments

4.1 Datasets

The PMC-VQA dataset [18] serves as the primary evaluation benchmark. The dataset provides a training split of 152,603 samples and a test split of 2,000 samples. All fine-tuning is performed exclusively on the training split; all reported accuracy metrics are computed on the held-out test split. Detailed dataset statistics are provided in Table 3 in Appendix A.4.

The answer distribution across options A–D is imbalanced in both splits, as shown in Figure 2. In the training set, options B and C together account for 73.5% of samples, with 35.6% and 37.8% for B and C respectively, while options A and D each represent less than 14%. The test set exhibits a similar but less pronounced skew, with B and C comprising 62.4% of samples, 31.9% and 30.5% for each, and A and D accounting for 21.9% and 15.8% respectively. This imbalance introduces an answer-position bias during fine-tuning, as the model learns to favor the more frequent answer positions.

For error analysis, we define nine question type categories based on the semantic content of the questions: *modality* for imaging technique identification, *anatomy* for anatomical structure identification, *color/label* for visual marker interpretation, *diagnosis* for disease or condition identification, *counting* for enumeration tasks, *comparison* for relational reasoning, *temporal* for staging or progression, *procedure* for treatment or intervention, and *other* for questions matching no category keywords. These categories are not provided by the PMC-VQA dataset; we define them heuristically using keyword matching on the question text to enable fine-grained error analysis. A question may match multiple categories. The complete keyword definitions are provided in Table 4 in Appendix A.5.

4.2 Baselines

We select baselines to cover both the published PMC-VQA leaderboard and representative compact open-source models. The published methods include PMC-CLIP [4], BLIP-2 [29], OpenFlamingo [58], LLaVA-Med [31], and MedICap-GPT-4 [18], which are chosen because they represent the best-reported results on the PMC-VQA benchmark. A trained variant, MedICaP-PMCVQA-GPT-4, is also included as the strongest supervised baseline. Additionally, we evaluate three compact open-source vision-language models under zero-shot inference to establish cross-architecture baselines: InternVL2-2B [39], SmolVLM2-2.2B [40], and Phi-3.5-vision [38], selected as current mainstream compact models suitable for portable device deployment. For our fine-tuning experiments, we use Qwen3-VL-2B-Instruct [19] and Qwen3-VL-4B-Instruct [19] as student models, with Qwen3-VL-235B-A22B-Instruct [19] as the teacher for chain-of-thought generation.

4.3 Implementation

Hardware and software specifications are provided in Appendix A.2. Fine-tuning applies LoRA with rank $r = 32$, scaling factor $\alpha = 64$, and dropout 0.05 to the query, key, value, and output projections. The training data is split into 51 chunks of approximately 3,000 samples each, processed sequentially with adapter weights carried forward. Each chunk is trained for 1 epoch, yielding an effective total

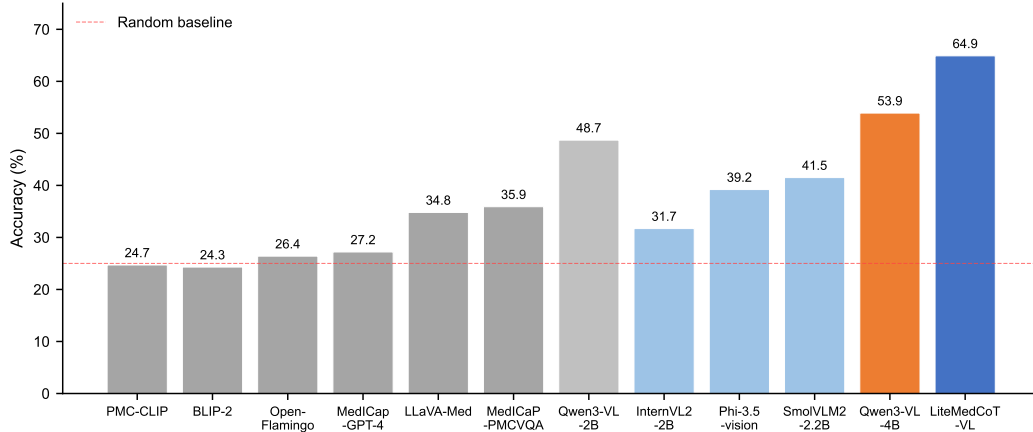


Figure 3: Accuracy of evaluated models on the PMC-VQA test set. The horizontal dashed line indicates the 25% random baseline for four-option multiple choice. Our LiteMedCoT-VL achieves 64.9%, outperforming all baselines.

of 1 epoch over the full dataset. Training uses the AdamW optimizer with a learning rate of 2×10^{-4} and 100 warmup steps under a linear schedule. The effective batch size is 8, achieved via per-device batch size 1 and gradient accumulation over 4 steps. Gradient norms are clipped to 1.0. All images are processed at their native resolution.

For chain-of-thought distillation, the teacher model Qwen3-VL-235B-A22B-Instruct generates explanations via API for 152,601 of 152,603 training samples, achieving 99.99% coverage. The average explanation length is 147 words with a median of 139 and a range of 5–438. Representative teacher explanations are provided in Appendix A.3.

Inference uses deterministic next-token logit scoring in bfloat16, with no sampling. To prevent test contamination, the teacher generates explanations exclusively for training split samples. This work uses publicly available benchmark data and does not involve new human-subject data collection.

5 Results

5.1 Comparison Results

Figure 3 reports accuracy for all evaluated models on the PMC-VQA test set; the full numerical data are provided in Table 5 in Appendix A.6. LiteMedCoT-VL achieves 64.9% accuracy, outperforming all published baselines. The base Qwen3-VL-2B achieves 48.7% without fine-tuning. The fine-tuned 2B model exceeds the zero-shot Qwen3-VL-4B at 53.9% by 11.0 percentage points. The zero-shot SmolVLM2-2.2B achieves 41.5%, already surpassing all published baselines. InternVL2-2B scores 31.7% zero-shot.

The published baseline numbers, from PMC-CLIP through MedICaP-PMCVQA-GPT-4, are taken from [18] and were obtained under different prompt designs and inference protocols. The compact open-source models are evaluated under our standardized deterministic PPL scoring protocol. Bootstrap 95% confidence intervals with 10,000 resamples for our evaluated models are: Qwen3-VL-2B 48.7% [46.6, 50.9], Qwen3-VL-4B 53.8% [51.6, 56.0], InternVL2-2B 31.7% [29.6, 33.8], SmolVLM2-2.2B 41.4% [39.3, 43.5], Phi-3.5-vision 39.1% [37.0, 41.3]. Head-to-head comparison of all methods under matched inference protocols remains desirable but is constrained by the availability of model weights and computational resources.

5.2 Ablation Study

Table 1 presents the ablation results comparing different training configurations. The base Qwen3-VL-2B achieves 48.7% with default settings. Fine-tuning with answer-only supervision and no

Table 1: Ablation of training configurations on Qwen3-VL-2B. Starting from the default 48.7%, no-caption fine-tuning, caption-aware training, and chain-of-thought distillation are applied incrementally. Each stage adds a supervision signal, with reasoning distillation providing the largest gain.

Configuration	Accuracy	Δ
Qwen3-VL-2B	48.7	–
+ no-caption fine-tuning	54.2	+5.5
+ caption-aware training	60.5	+6.3
+ CoT distillation (LiteMedCoT-VL)	64.9	+4.4

caption improves performance to 54.2%. Adding caption-aware training further increases accuracy to 60.5%. The full LiteMedCoT-VL pipeline, which injects chain-of-thought reasoning from Qwen3-VL-235B-A22B-Instruct into the training data, achieves 64.9%, a 4.4 percentage point improvement over caption-aware training alone. Each configuration is evaluated deterministically on the same 2,000-sample test set with fixed inference settings.

Fine-tuning introduces an answer-position bias: the fine-tuned model achieves higher accuracy on options B at 61.0% and C at 71.6%, compared to A at 36.6% and D at 31.1%. This pattern reflects the imbalanced answer distribution in the PMC-VQA training set, where B and C account for 73.5% of samples. The bias is less pronounced in the default Qwen3-VL-4B, which ranges from 45.1% to 58.9% across positions.

5.3 Visual Grounding Analysis

To assess whether the models genuinely rely on visual information, we conduct an image ablation study across all baseline models. Figure 4 presents the results of running inference with images removed, using only the question and options text. All models show substantial performance degradation when images are withheld. Qwen3-VL-2B drops from 48.7% to 32.9%, a 15.8pp decrease, and Qwen3-VL-4B drops from 53.9% to 36.5%, a 17.4pp decrease, confirming that both models leverage visual information for prediction. SmolVLM2-2.2B shows the largest drop of 19.6pp, while Phi-3.5-vision shows a more modest decrease of 6.9pp. The no-image accuracies for InternVL2-2B and SmolVLM2-2.2B fall to 21.9%, below the 25% random baseline, indicating that these models default to predicting the most frequent answer position when images are removed rather than exploiting textual cues. In contrast, Qwen3-VL-2B, Qwen3-VL-4B, and Phi-3.5-vision maintain no-image accuracies above the random baseline at 32.9%, 36.5%, and 32.3% respectively, suggesting some exploitation of textual cues within questions and answer options, consistent with findings from MIRAGE [50]. The exact numerical data are provided in Table 6 in Appendix A.7.

The fine-tuned variants, namely LiteMedCoT-VL, no-caption FT, and caption FT, are excluded from this ablation because the fine-tuning procedure itself may alter the model’s reliance on visual versus textual cues. Specifically, fine-tuning on answer-only supervision with imbalanced answer distributions can amplify position bias, confounding the interpretation of the no-image experiment.

5.4 Error Analysis by Question Type

To understand where chain-of-thought distillation yields the greatest gains, we categorize test questions by type using keyword matching; definitions are provided in Appendix A.5. Figure 5 reports results for all evaluated models; complete numerical data appear in Table 7 in Appendix A.8. Among the zero-shot baselines, Qwen3-VL-4B consistently outperforms the smaller models, while InternVL2-2B shows the weakest performance across most categories. Fine-tuning yields the largest gains on *anatomy* at +24.7pp and *color/label* at +19.5pp, both categories that require visual interpretation of imaging features. The *procedure* category achieves the highest accuracy across all configurations, ranging from 35.8% to 82.1%. The *comparison* category remains the most challenging for most models, with InternVL2-2B and SmolVLM2-2.2B scoring below 30%. The fine-tuned model improves accuracy across all answer positions, with position A showing the largest gain of 22.7pp and positions B, C, and D each improving by 13–16pp.

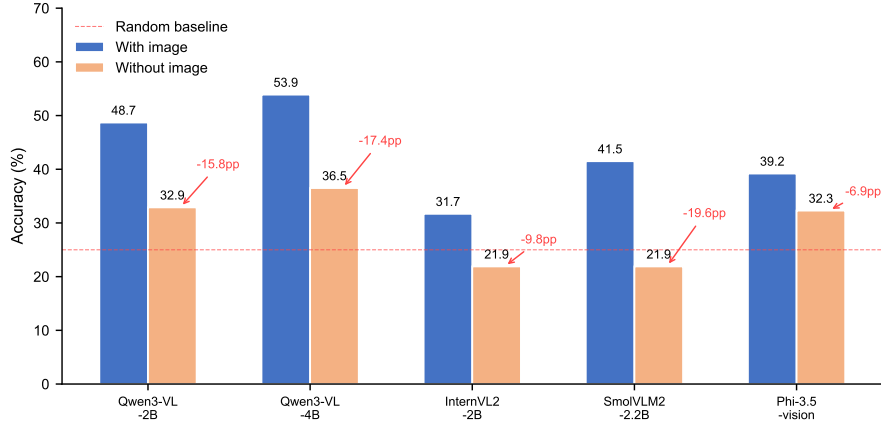


Figure 4: Image ablation results across all baseline models. Removing images causes substantial accuracy drops for all models, confirming genuine visual reliance. Fine-tuned variants are excluded because fine-tuning may alter the model’s reliance on visual versus textual cues.

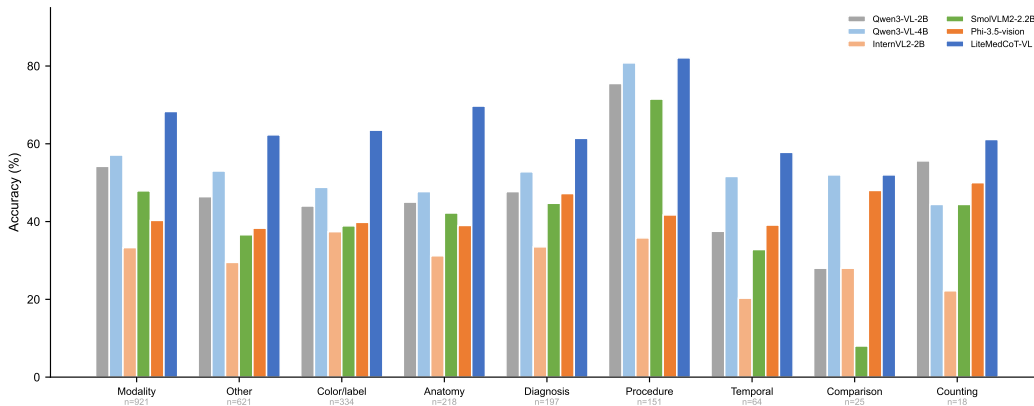


Figure 5: Per-category accuracy on the PMC-VQA test set. Sample sizes per category are shown below the x-axis. LiteMedCoT-VL achieves the largest gains on anatomy and color/label relative to the 2B default.

6 Discussion

The results demonstrate that chain-of-thought distillation from a 235B teacher improves a 2B student model by 16.2 percentage points on PMC-VQA, with 4.4pp of that gain attributable specifically to CoT distillation beyond caption-aware training. This finding aligns with the broader trend of reasoning transfer in medical VQA, though the mechanisms differ across approaches. Step-CoT [13] leverages expert-curated structured annotations with graph-based focusing, achieving gains through annotation quality. CheXthought [14] shows that radiologist-authored traces with visual attention hints surpass VLM-generated CoT in factual accuracy. MedE2 [17] combines demonstration elicitation with Direct Preference Optimization. Trajectory-aware GRPO [15] applies process rewards based on reasoning-step similarity, and CARE [16] decomposes VQA into specialized sub-modules trained with reinforcement learning. LiteMedCoT-VL offers a simpler, single-stage recipe that does not require expert annotations or multi-stage pipelines, though it does not match the structured grounding of agentic frameworks like CARE. The trade-off between recipe simplicity and reasoning fidelity warrants further investigation.

The 11.0 percentage point gap between LiteMedCoT-VL at 64.9% and the zero-shot Qwen3-VL-4B at 53.9% indicates that reasoning capability, rather than parameter count alone, drives performance

on this benchmark. The caption-aware results further illuminate this finding: the 6.3pp improvement from caption inclusion, from 54.2% to 60.5%, suggests that textual context complements visual features, analogous to how a radiology report supplements a clinician’s direct image interpretation. However, this gain may partly reflect shortcut learning from caption–answer correlations in the training data rather than genuine multimodal integration.

The answer-position bias observed after fine-tuning, with accuracy ranging from 31.1% for option D to 71.6% for option C, reflects the imbalanced answer distribution in the PMC-VQA training set. This bias is less pronounced in the default Qwen3-VL-4B at 45.1%–58.9%, suggesting that fine-tuning amplifies sensitivity to label frequency. Mitigation strategies such as balanced sampling, label smoothing, or focal loss merit exploration in future iterations.

7 Limitations

Evaluation is limited to PMC-VQA and the Qwen3-VL model family. Cross-dataset generalization to SLAKE [32], PathVQA [33], and VQA-RAD [59], and cross-architecture distillation remain open. The single-image evaluation does not capture multi-image clinical reasoning [57] or resolution sensitivity [56].

The fine-tuned variants are excluded from the no-image ablation because fine-tuning may alter the model’s reliance on visual versus textual cues. More rigorous grounding verification of the distilled model remains necessary. The counterfactual evaluation framework of Zafar et al. [54], which introduces VRS, IS, and HVRR metrics using real, blank, and shuffled images, provides a principled approach. HALT-MedVQA [55] stress tests using fake questions, “None of the Above” choices, and image swaps offer complementary diagnostic signals. The entropy-guided regrounding of MedVR [51], the iterative think-act-rethink chains of ViTAR [52], and the causal deconfounding framework of DCI [53] provide additional avenues for grounding verification.

All results are reported from single training runs. The deterministic inference protocol eliminates decoding variance, but training variance from data ordering and random initialization is not quantified. The published baseline numbers are taken from prior work under different inference protocols, limiting the fairness of direct comparison.

We have not measured latency, memory footprint, throughput, or energy consumption on representative portable hardware. Quantization effects on accuracy are also unexplored. These measurements are necessary to substantiate practical deployment claims.

All experiments use curated benchmark data under offline evaluation. No clinical deployment validation or expert review has been conducted. Teacher-generated explanations are assessed only by coverage and length statistics, not by clinical expert evaluation. The faithfulness of distilled reasoning chains to the teacher’s actual visual attention remains an open question; CheXthought [14] demonstrates that expert-verified traces with visual attention annotations yield more grounded reasoning, suggesting that lightweight clinician audits of teacher outputs could improve distillation quality.

8 Conclusion

This work demonstrates that chain-of-thought knowledge distillation from a 235B teacher can improve the performance of compact vision-language models on medical visual question answering. LiteMedCoT-VL achieves 64.9% on PMC-VQA, exceeding the 4B model at 53.9% and all published baselines. The distillation from Qwen3-VL-235B-A22B-Instruct improves student accuracy from 48.7% to 64.9%, indicating that reasoning capability transfers effectively across model scales. A 2B model with LoRA adaptation can outperform a model with twice the parameters, reducing the compute and memory requirements for resource-constrained clinical settings. Visual grounding verification, multi-dataset evaluation, efficiency measurements on portable hardware, and clinical validation remain necessary to establish the reliability of these findings for deployment.

A Appendix

A.1 System Prompts

The complete prompts used in the pipeline are reproduced below, corresponding to the three prompt families described in Section 3.

No-Caption Inference Prompt

System prompt

You are a professional medical scientist. Answer the choice question based strictly on the image.

STRICT OUTPUT FORMAT:

1. You MUST output ONLY a single uppercase letter: A, B, C, or D.
2. DO NOT output the full option text.
3. DO NOT output phrases like 'The answer is'.
4. NO explanation, NO reasoning, NO punctuation.

Example Output:

A

User message format

Question: [question text]

Options:

- A. [option A]
- B. [option B]
- C. [option C]
- D. [option D]

Caption-Aware Inference Prompt

System prompt

You are a professional medical scientist. Answer the choice question based strictly on the image and the caption.

STRICT OUTPUT FORMAT:

1. You MUST output ONLY a single uppercase letter: A, B, C, or D.
2. DO NOT output the full option text.
3. DO NOT output phrases like 'The answer is'.
4. NO explanation, NO reasoning, NO punctuation.

Example Output:

A

User message format

Image caption: [caption text]

Question: [question text]

Options:

- A. [option A]
- B. [option B]
- C. [option C]
- D. [option D]

Chain-of-Thought Training Prompt

This prompt is used during SFT training with distilled explanations from the teacher model (Section 3).

System prompt

You are a professional medical scientist. Answer the choice

question based strictly on the image.

OUTPUT FORMAT:

1. First, provide your reasoning and analysis based on the image.
2. Then output on a new line exactly: Answer: <LETTER>.
3. The letter MUST be A, B, C, or D.

Example Output:

Explanation: [Your detailed analysis of the image findings]

Answer: A

A.2 Hardware and Software Setup

Table 2 specifies the hardware and software environment used for all experiments (Section 4).

Table 2: Hardware and software specifications.

Component	Specification
GPU	NVIDIA GeForce RTX 5090, 32 GB VRAM
CPU	25 vCPU Intel Xeon Platinum 8470Q
RAM	120 GB
OS	Ubuntu 22.04
Python	3.12
PyTorch	2.8.0
CUDA	12.8
Transformers	4.45+
Attention	Flash Attention 2

A.3 Teacher Chain-of-Thought Examples

The following examples illustrate the quality and diversity of chain-of-thought explanations generated by the teacher model Qwen3-VL-235B-A22B-Instruct for PMC-VQA training samples (Section 3).

Example 1: Color identification

Question: What color is used to label the Golgi complexes in the image?

Answer: B (Red)

Teacher explanation: The image depicts a three-dimensional reconstruction of a eukaryotic cell, with various organelles labeled using distinct colors. The nucleus is clearly visible in the center, rendered in light blue, which is a common color choice for nuclear labeling in such visualizations. Surrounding the nucleus, the green structures represent the endoplasmic reticulum (ER), identifiable by their extensive network and tubular morphology. The Golgi complex, located near the nucleus and typically positioned adjacent to the ER, is shown as a cluster of small, stacked, red-colored vesicles. This red labeling corresponds to the Golgi apparatus, which is often highlighted in red in fluorescent microscopy or 3D reconstructions to distinguish it from other organelles. Therefore, based on the visual features—specifically the red-stained vesicular structure adjacent to the nucleus and ER—the correct answer is B: Red.

Example 2: Modality identification

Question: What type of imaging was used to demonstrate acute infarct?

Answer: C (Diffusion weighted image)

Teacher explanation: The image shows two axial brain slices with hyperintense (bright) lesions in the cerebral cortex and subcortical regions, particularly prominent in the right hemisphere. These bright signals are characteristic of restricted diffusion, which is a hallmark of acute ischemic stroke. Diffusion-weighted imaging (DWI) is highly sensitive to cytotoxic edema that occurs within minutes of ischemia, making it the most effective MRI sequence for detecting acute infarcts. The presence of these bright lesions on DWI, coupled with the typical location and acute clinical context implied

by the question, confirms that the imaging modality used was diffusion-weighted imaging. Time-of-flight MR (A) is used for vascular imaging, not tissue infarct detection; DSA (B) is an invasive angiographic technique primarily for evaluating vessel patency, not parenchymal changes. Therefore, the correct answer is C: Diffusion weighted image.

Example 3: Anatomical structure identification

Question: What is shown in the image?

Answer: C (Transverse section anatomy of the storage root)

Teacher explanation: The image displays a transverse (cross) section of a plant structure, characterized by a central vascular bundle surrounded by parenchyma cells, which is typical of a storage root. The presence of a large central stele with phloem and xylem arranged in a radial pattern, along with thick-walled storage parenchyma cells, indicates a modified root adapted for storage. This anatomy is consistent with a transverse section of a storage root, such as those found in carrots or beets. The two upward-pointing arrows likely highlight the vascular bundles, further supporting the identification of a root structure. The overall organization lacks the epidermis and stomata seen in leaves, and the arrangement differs from stem anatomy, which typically shows vascular bundles in a ring or scattered pattern. Therefore, the correct answer is C: Transverse section anatomy of the storage root.

A.4 Dataset Statistics

Table 3 reports the PMC-VQA dataset statistics referenced in Section 4.

Table 3: PMC-VQA dataset statistics by answer label.

	Training	Test
Total samples	152,603	2,000
Answer A	21,023	437
Answer B	54,348	638
Answer C	57,685	610
Answer D	19,547	315

A.5 Question Type Definitions

Table 4 defines the nine question categories used in the error analysis (Section 5). Categories are assigned by keyword matching on the question text; a question may match multiple categories.

Table 4: Question type categories and their keyword definitions.

Category	Keywords
Modality	imaging, modality, technique, scan, MRI, CT, X-ray, radiograph, ultrasound, microscope, photograph, fluorescence, PET, SPECT, endoscope, histology, pathology
Anatomy	organ, structure, anatomy, region, location, lobe, artery, vein, nerve, bone, muscle, tissue, cell, membrane, cortex, nucleus, ventricle
Color/label	color, label, labelled, labeled, arrow, highlight, indicate, mark, point
Diagnosis	diagnosis, disease, condition, pathological, abnormal, finding, appearance, suggest, consistent with, likely
Counting	how many, number of, count, quantity, multiple
Comparison	compare, difference, differ, similar, versus, vs, than, more, less, larger, smaller
Temporal	stage, phase, progress, develop, time, course, acute, chronic, early, late, before, after
Procedure	procedure, treatment, surgery, intervention, therapy, approach, technique, method
Other	no keyword match

A.6 Comparison Results

Table 5 provides the exact accuracy values for all evaluated models corresponding to Figure 3 (Section 5).

Table 5: Accuracy of all evaluated models on the PMC-VQA test set.

Model	Accuracy (%)
PMC-CLIP	24.7
BLIP-2	24.3
Open-Flamingo	26.4
MediCap-GPT-4	27.2
LLaVA-Med	34.8
MediCaP-PMCVQA-GPT-4	35.9
Qwen3-VL-2B	48.7
InternVL2-2B	31.7
Phi-3.5-vision	39.2
SmolVLM2-2.2B	41.5
Qwen3-VL-4B	53.9
LiteMedCoT-VL	64.9

A.7 Ablation and Visual Grounding

Table 6 provides the image ablation accuracy corresponding to Figure 4 (Section 5).

Table 6: Image ablation accuracy with and without images for all baseline models.

Model	With image (%)	Without image (%)	Δ (pp)
Qwen3-VL-2B	48.7	32.9	-15.8
Qwen3-VL-4B	53.9	36.5	-17.4
InternVL2-2B	31.7	21.9	-9.8
SmolVLM2-2.2B	41.5	21.9	-19.6
Phi-3.5-vision	39.2	32.3	-6.9

A.8 Error Analysis Data

Table 7 provides per-category accuracy values corresponding to Figure 5 in the main text.

Table 7: Per-category accuracy on the PMC-VQA test set.

Model	Modality <i>n</i> =921	Other <i>n</i> =621	Color/label <i>n</i> =334	Anatomy <i>n</i> =218	Diagnosis <i>n</i> =197	Procedure <i>n</i> =151	Temporal <i>n</i> =64	Comparison <i>n</i> =25	Counting <i>n</i> =18
Qwen3-VL-2B	54.2	46.4	44.0	45.0	47.7	75.5	37.5	28.0	55.6
Qwen3-VL-2B-NoCaption	60.6	52.0	47.0	53.7	52.8	79.5	42.2	28.0	44.4
Qwen3-VL-2B-Caption	63.8	59.1	53.0	57.3	62.4	73.5	53.1	48.0	66.7
Qwen3-VL-4B	57.1	53.0	48.8	47.7	52.8	80.8	51.6	52.0	44.4
InternVL2-2B	33.3	29.5	37.4	31.2	33.5	35.8	20.3	28.0	22.2
SmolVLM2-2.2B	47.9	36.6	38.9	42.2	44.7	71.5	32.8	8.0	44.4
Phi-3.5-vision	40.3	38.3	39.8	39.0	47.2	41.7	39.1	48.0	50.0
LiteMedCoT-VL	68.3	62.3	63.5	69.7	61.4	82.1	57.8	52.0	61.1

References

- [1] S Kevin Zhou, Hayit Greenspan, Christos Davatzikos, James S Duncan, Bram Van Ginneken, Anant Madabhushi, Jerry L Prince, Daniel Rueckert, and Ronald M Summers. A review of deep learning in medical imaging: Imaging traits, technology trends, case studies with progress highlights, and future promises. *Proceedings of the IEEE*, 109(5):820–838, 2021.
- [2] Masayuki Tsuneki. Deep learning models in medical image analysis. *Journal of Oral Biosciences*, 64(3):312–320, 2022.
- [3] Yuxiao Gao, Yang Jiang, Yanhong Peng, Fujiang Yuan, Xinyue Zhang, and Jianfeng Wang. Medical image segmentation: A comprehensive review of deep learning-based methods. *Tomography*, 11(5):52, 2025.
- [4] Alec Radford, Jong Wook Kim, Chris Hallacy, Aditya Ramesh, Gabriel Goh, Sandhini Agarwal, Girish Sastry, Amanda Askell, Pamela Mishkin, Jack Clark, et al. Learning transferable visual models from natural language supervision. In *International conference on machine learning*, pages 8748–8763. PMLR, 2021.
- [5] Chao Jia, Yinfei Yang, Ye Xia, Yi-Ting Chen, Zarana Parekh, Hieu Pham, Quoc Le, Yun-Hsuan Sung, Zhen Li, and Tom Duerig. Scaling up visual and vision-language representation learning with noisy text supervision. In *International conference on machine learning*, pages 4904–4916. PMLR, 2021.
- [6] Gemini Team, Petko Georgiev, Ving Ian Lei, Ryan Burnell, Libin Bai, Anmol Gulati, Garrett Tanzer, Damien Vincent, Zhufeng Pan, Shibo Wang, et al. Gemini 1.5: Unlocking multimodal understanding across millions of tokens of context. *arXiv preprint arXiv:2403.05530*, 2024.
- [7] Jingyi Zhang, Jiaying Huang, Sheng Jin, and Shijian Lu. Vision-language models for vision tasks: A survey. *IEEE transactions on pattern analysis and machine intelligence*, 46(8):5625–5644, 2024.
- [8] Peng Wang, Wenpeng Lu, Chunlin Lu, Ruoxi Zhou, Min Li, and Libo Qin. Large language model for medical images: A survey of taxonomy, systematic review, and future trends. *Big Data Mining and Analytics*, 8(2):496, 2025.
- [9] Chunyu Liu, Yixiao Jin, Zhouyu Guan, Tingyao Li, Yiming Qin, Bo Qian, Zehua Jiang, Yilan Wu, Xiangning Wang, Ying Feng Zheng, et al. Visual–language foundation models in medicine. *The Visual Computer*, 41(4):2953–2972, 2025.
- [10] Bin Sheng, Zhouyu Guan, Lee-Ling Lim, Zehua Jiang, Nestoras Mathioudakis, Jiajia Li, Ruhao Liu, Yuqian Bao, Yong Mong Bee, Ya-Xing Wang, et al. Large language models for diabetes care: Potentials and prospects. *Science bulletin*, 69(5):583–588, 2024.
- [11] Jianping Gou, Baosheng Yu, Stephen J Maybank, and Dacheng Tao. Knowledge distillation: A survey. *International journal of computer vision*, 129(6):1789–1819, 2021.
- [12] Amir M Mansourian, Rozhan Ahmadi, Masoud Ghafouri, Amir Mohammad Babaei, Elaheh Badali Golezani, Zeynab Yasamani Ghamchi, Vida Ramezani, Alireza Taherian, Kimia Dinashi, Amirali Miri, et al. A comprehensive survey on knowledge distillation. *arXiv preprint arXiv:2503.12067*, 2025.
- [13] Lin Fan, Yafei Ou, Zhipeng Deng, Pengyu Dai, Hou Chongxian, Jiale Yan, Yaqian Li, Kaiwen Long, Xun Gong, Masayuki Ikebe, et al. Step-cot: Stepwise visual chain-of-thought for medical visual question answering. *arXiv preprint arXiv:2603.13878*, 2026.
- [14] Sonali Sharma, Jin Long, George Shih, Sarah Eid, Christian Bluethgen, Francine L Jacobson, Emily B Tsai, Ahmed M Alaa, Curtis P Langlotz, Global Radiology Consortium, et al. Chexthought: A global multimodal dataset of clinical chain-of-thought reasoning and visual attention for chest x-ray interpretation. *arXiv preprint arXiv:2604.26288*, 2026.
- [15] Halil Ibrahim Gulluk and Olivier Gevaert. Improving medical vqa through trajectory-aware process supervision. *arXiv preprint arXiv:2605.04064*, 2026.

- [16] Yuexi Du, Jinglu Wang, Shujie Liu, Nicha C Dvornek, and Yan Lu. Care: Towards clinical accountability in multi-modal medical reasoning with an evidence-grounded agentic framework. *arXiv preprint arXiv:2603.01607*, 2026.
- [17] Zhongzhen Huang, Linjie Mu, Yakun Zhu, Xiangyu Zhao, Shaoting Zhang, and Xiaofan Zhang. Elicit and enhance: Advancing multimodal reasoning in medical scenarios. *arXiv preprint arXiv:2505.23118*, 2025.
- [18] Xiaoman Zhang, Chaoyi Wu, Ziheng Zhao, Weixiong Lin, Ya Zhang, Yanfeng Wang, and Weidi Xie. Pmc-vqa: Visual instruction tuning for medical visual question answering. *arXiv preprint arXiv:2305.10415*, 2023.
- [19] Shuai Bai, Yuxuan Cai, Ruizhe Chen, Keqin Chen, Xionghui Chen, Zesen Cheng, Lianghao Deng, Wei Ding, Chang Gao, Chunjiang Ge, et al. Qwen3-vl technical report. *arXiv preprint arXiv:2511.21631*, 2025.
- [20] Sandra Jardim, João António, and Carlos Mora. Image thresholding approaches for medical image segmentation-short literature review. *Procedia Computer Science*, 219:1485–1492, 2023.
- [21] Mohammad R Salmanpour, Somayeh Sadat Mehrnia, Sajad Jabarzadeh Ghandilu, Zhino Safahi, Sonya Falahati, Shahram Taeb, Ghazal Mousavi, Mehdi Maghsudi, Ahmad Sharifabrizi, Ilker Hacihaliloglu, et al. Handcrafted vs. deep radiomics vs. fusion vs. deep learning: A comprehensive review of machine learning-based cancer outcome prediction in pet and spect imaging. *Journal of Imaging Informatics in Medicine*, pages 1–50, 2026.
- [22] Chao Chen, Nor Ashidi Mat Isa, and Xin Liu. A review of convolutional neural network based methods for medical image classification. *Computers in biology and medicine*, 185:109507, 2025.
- [23] Carina Albuquerque, Roberto Henriques, and Mauro Castelli. Deep learning-based object detection algorithms in medical imaging: Systematic review. *Heliyon*, 11(1), 2025.
- [24] Ibomoiye Domor Mienye, Theo G Swart, George Obaido, Matt Jordan, and Philip Ilono. Deep convolutional neural networks in medical image analysis: A review. *Information*, 16(3):195, 2025.
- [25] Jieneng Chen, Yongyi Lu, Qihang Yu, Xiangde Luo, Ehsan Adeli, Yan Wang, Le Lu, Alan L Yuille, and Yuyin Zhou. Transunet: Transformers make strong encoders for medical image segmentation. *arXiv preprint arXiv:2102.04306*, 2021.
- [26] Hu Cao, Yueyue Wang, Joy Chen, Dongsheng Jiang, Xiaopeng Zhang, Qi Tian, and Manning Wang. Swin-unet: Unet-like pure transformer for medical image segmentation. In *European conference on computer vision*, pages 205–218. Springer, 2022.
- [27] Kelei He, Chen Gan, Zhuoyuan Li, Islem Rekik, Zihao Yin, Wen Ji, Yang Gao, Qian Wang, Junfeng Zhang, and Dinggang Shen. Transformers in medical image analysis. *Intelligent Medicine*, 3(1):59–78, 2023.
- [28] Wenjie Dong, Shuhao Shen, Yuqiang Han, Tao Tan, Jian Wu, and Hongxia Xu. Generative models in medical visual question answering: A survey. *Applied Sciences*, 15(6):2983, 2025.
- [29] Junnan Li, Dongxu Li, Silvio Savarese, and Steven Hoi. Blip-2: Bootstrapping language-image pre-training with frozen image encoders and large language models. In *International conference on machine learning*, pages 19730–19742. PMLR, 2023.
- [30] Amanpreet Singh, Ronghang Hu, Vedanuj Goswami, Guillaume Couairon, Wojciech Galuba, Marcus Rohrbach, and Douwe Kiela. Flava: A foundational language and vision alignment model. In *Proceedings of the IEEE/CVF conference on computer vision and pattern recognition*, pages 15638–15650, 2022.
- [31] Chunyuan Li, Cliff Wong, Sheng Zhang, Naoto Usuyama, Haotian Liu, Jianwei Yang, Tristan Naumann, Hoifung Poon, and Jianfeng Gao. Llava-med: Training a large language-and-vision assistant for biomedicine in one day. *Advances in Neural Information Processing Systems*, 36: 28541–28564, 2023.

- [32] Bo Liu, Li-Ming Zhan, Li Xu, Lin Ma, Yan Yang, and Xiao-Ming Wu. Slake: A semantically-labeled knowledge-enhanced dataset for medical visual question answering. In *2021 IEEE 18th international symposium on biomedical imaging (ISBI)*, pages 1650–1654. IEEE, 2021.
- [33] Xuehai He, Yichen Zhang, Luntian Mou, Eric Xing, and Pengtao Xie. Pathvqa: 30000+ questions for medical visual question answering. *arXiv preprint arXiv:2003.10286*, 2020.
- [34] Asma Ben Abacha, Mourad Sarrouiti, Dina Demner-Fushman, Sadid A Hasan, and Henning Müller. Overview of the vqa-med task at imageclef 2021: Visual question answering and generation in the medical domain. In *Proceedings of the CLEF 2021 Conference and Labs of the Evaluation Forum-working notes*. 21-24 September 2021, 2021.
- [35] Kaixiang Zheng and En-Hui Yang. Knowledge distillation based on transformed teacher matching. *arXiv preprint arXiv:2402.11148*, 2024.
- [36] Mengyang Yuan, Bo Lang, and Fengnan Quan. Student-friendly knowledge distillation. *Knowledge-Based Systems*, 296:111915, 2024.
- [37] Muyu Wang, Shiyu Fan, Yichen Li, Binyu Gao, Zhongrang Xie, and Hui Chen. Robust multi-modal fusion architecture for medical data with knowledge distillation. *Computer methods and programs in biomedicine*, 260:108568, 2025.
- [38] Marah Abdin, Jyoti Aneja, Hany Awadalla, Ahmed Awadallah, Ammar Ahmad Awan, Nguyen Bach, Amit Bahree, Arash Bakhtiari, Jianfeng Bao, Harkirat Behl, et al. Phi-3 technical report: A highly capable language model locally on your phone. *arXiv preprint arXiv:2404.14219*, 2024.
- [39] Zhe Chen, Weiyun Wang, Hao Tian, Shenglong Ye, Zhangwei Gao, Erfei Cui, Wenwen Tong, Kongzhi Hu, Jiapeng Luo, Zheng Ma, et al. How far are we to gpt-4v? closing the gap to commercial multimodal models with open-source suites. *Science China Information Sciences*, 67(12):220101, 2024.
- [40] Andrés Marafioti, Orr Zohar, Miquel Farré, Merve Noyan, Elie Bakouch, Pedro Cuenca, Cyril Zakka, Loubna Ben Allal, Anton Lozhkov, Nouamane Tazi, et al. Smolvlm: Redefining small and efficient multimodal models. *arXiv preprint arXiv:2504.05299*, 2025.
- [41] Yue Jiang, Jiawei Chen, Dingkan Yang, Mingcheng Li, Shunli Wang, Tong Wu, Ke Li, and Lihua Zhang. Comt: Chain-of-medical-thought reduces hallucination in medical report generation. In *ICASSP 2025-2025 IEEE International Conference on Acoustics, Speech and Signal Processing (ICASSP)*, pages 1–5. IEEE, 2025.
- [42] Namgyu Ho, Laura Schmid, and Se-Young Yun. Large language models are reasoning teachers. In *Proceedings of the 61st annual meeting of the association for computational linguistics (volume 1: long papers)*, pages 14852–14882, 2023.
- [43] Xuezhi Wang, Jason Wei, Dale Schuurmans, Quoc Le, Ed Chi, Sharan Narang, Aakanksha Chowdhery, and Denny Zhou. Self-consistency improves chain of thought reasoning in language models. *arXiv preprint arXiv:2203.11171*, 2022.
- [44] Edward J Hu, Yelong Shen, Phillip Wallis, Zeyuan Allen-Zhu, Yuanzhi Li, Shean Wang, Liang Wang, Weizhu Chen, et al. Lora: Low-rank adaptation of large language models. *Iclr*, 1(2):3, 2022.
- [45] Neil Houlsby, Andrei Giurgiu, Stanislaw Jastrzebski, Bruna Morrone, Quentin De Laroussilhe, Andrea Gesmundo, Mona Attariyan, and Sylvain Gelly. Parameter-efficient transfer learning for nlp. In *International conference on machine learning*, pages 2790–2799. PMLR, 2019.
- [46] Xiang Lisa Li and Percy Liang. Prefix-tuning: Optimizing continuous prompts for generation. In *Proceedings of the 59th Annual Meeting of the Association for Computational Linguistics and the 11th International Joint Conference on Natural Language Processing (Volume 1: Long Papers)*, pages 4582–4597, 2021.

- [47] Yuning Mao, Lambert Mathias, Rui Hou, Amjad Almahairi, Hao Ma, Jiawei Han, Scott Yih, and Madian Khabsa. Unipelt: A unified framework for parameter-efficient language model tuning. In *Proceedings of the 60th Annual Meeting of the Association for Computational Linguistics (Volume 1: Long Papers)*, pages 6253–6264, 2022.
- [48] Yuren Mao, Yuhang Ge, Yijiang Fan, Wenyi Xu, Yu Mi, Zhonghao Hu, and Yunjun Gao. A survey on lora of large language models. *Frontiers of Computer Science*, 19(7):197605, 2025.
- [49] Egor Volkov, Vadim Sechin, and Alexey Averkin. Visual-language model fine-tuning via lora for structured medical reports generating for lung x-ray scans. In *2025 XXVIII International Conference on Soft Computing and Measurements (SCM)*, pages 438–442. IEEE, 2025.
- [50] Mohammad Asadi, Jack W O’Sullivan, Fang Cao, Tahoura Nedae, Kamyar Fardi, Fei-Fei Li, Ehsan Adeli, and Euan Ashley. Mirage the illusion of visual understanding. *arXiv preprint arXiv:2603.21687*, 2026.
- [51] Zheng Jiang, Heng Guo, Chengyu Fang, Changchen Xiao, Xinyang Hu, Lifeng Sun, and Minfeng Xu. Medvr: Annotation-free medical visual reasoning via agentic reinforcement learning. *arXiv preprint arXiv:2604.08203*, 2026.
- [52] Kaitao Chen, Shaohao Rui, Yankai Jiang, Jiamin Wu, Qihao Zheng, Chunfeng Song, Xiaosong Wang, Mu Zhou, and Mianxin Liu. Think twice to see more: Iterative visual reasoning in medical vlms. *arXiv preprint arXiv:2510.10052*, 2025.
- [53] Zibo Xu, Qiang Li, Ke Lu, Jin Wang, Weizhi Nie, and Yuting Su. Dual causal inference: Integrating backdoor adjustment and instrumental variable learning for medical vqa. *arXiv preprint arXiv:2604.20306*, 2026.
- [54] Anas Zafar, Leema Krishna Murali, and Ashish Vashtist. Beyond accuracy: Evaluating visual grounding in multimodal medical reasoning. *arXiv preprint arXiv:2603.03437*, 2026.
- [55] Jinge Wu, Yunsoo Kim, and Honghan Wu. Hallucination benchmark in medical visual question answering. *arXiv preprint arXiv:2401.05827*, 2024.
- [56] Liangyu Chen, James Burgess, Jeffrey J Nirschl, Orr Zohar, and Serena Yeung-Levy. The impact of image resolution on biomedical multimodal large language models. *arXiv preprint arXiv:2510.18304*, 2025.
- [57] Suhao Yu, Haojin Wang, Juncheng Wu, Luyang Luo, Jingshen Wang, Cihang Xie, Pranav Rajpurkar, Carl Yang, Yang Yang, Kang Wang, et al. Medframeqa: A multi-image medical vqa benchmark for clinical reasoning. *arXiv preprint arXiv:2505.16964*, 2025.
- [58] Anas Awadalla, Irena Gao, Josh Gardner, Jack Hessel, Yusuf Hanafy, Wanrong Zhu, Kalyani Marathe, Yonatan Bitton, Samir Gadre, Shiori Sagawa, et al. Openflamingo: An open-source framework for training large autoregressive vision-language models. *arXiv preprint arXiv:2308.01390*, 2023.
- [59] Jason J Lau, Soumya Gayen, Asma Ben Abacha, and Dina Demner-Fushman. A dataset of clinically generated visual questions and answers about radiology images. *Scientific data*, 5(1):180251, 2018.